

Coherent control of spatial and angular Goos-Hänchen shifts in a metal-clad waveguide structureRen-Gang Wan^{1,2,*} and M. Suhail Zubairy^{2,†}¹*School of Physics and Information Technology, Shaanxi Normal University, Xi'an 710062, China*²*Institute for Quantum Science and Engineering (IQSE) and Department of Physics and Astronomy, Texas A&M University, College Station, Texas 77843-4242, USA*

(Received 25 November 2019; accepted 3 February 2020; published 25 February 2020)

A metal-clad waveguide backed by a coherent atomic medium is proposed to achieve tunable giant spatial and angular Goos-Hänchen (GH) shifts. With a metal layer of appropriate thickness, a large GH shift can occur simultaneously for transverse-magnetic- and transverse-electric-polarized light beams when the waveguide modes are resonantly excited. The phase change and dip slope of the reflection coefficient around the resonance angle are closely related to the system's internal damping, which depends on the absorption of the medium. Then based on the quantum coherence effect, the spatial and angular shifts can be greatly enhanced by adjusting the parameters of the atomic system. The lateral displacement can also be switched from positive to negative or vice versa via coherent control of the absorption by the medium. Moreover, the dependence of the resonance angle of the guided mode on the refractive index makes the peak position of GH shifts tunable. The proposed scheme provides more flexibility for manipulating the spatial and the angular GH shifts, and it has potential applications in optical switches, beam steering, etc.

DOI: [10.1103/PhysRevA.101.023837](https://doi.org/10.1103/PhysRevA.101.023837)**I. INTRODUCTION**

Goos and Hänchen (GH) observed the lateral displacement of a light beam totally reflected from the boundary between two dielectric media [1]. Artmann explained this effect by considering a beam with finite width of which the plane-wave components have different transverse wave vectors. Therefore, the reflected beam is a superposition of all the components, with each component undergoing a different phase change. As a result, a longitudinal shift occurs in the plane of incidence [2]. In addition to the spatial GH shift, there is also a shift in the reflection angle that results from the different reflective coefficient for each plane-wave component [3,4]. In the past decades, the spatial and angular GH shifts have been investigated extensively in both theory and experiment due to their potential applications in optical switching [5], optical sensing [6–8], and beam steering [9].

In the scheme of total reflection with a single dielectric interface, the GH shift is usually positive and small (on the order of a wavelength). Therefore, much attention has been paid to achieving negative and large lateral displacement. Different materials and structures can be employed to enhance the GH effect, such as single- or double-negative materials [10–12], a dielectric slab [13,14], absorbing and active media [15,16], photonic crystals [17,18], graphene [19,20], a double-prism configuration [21], surface plasmon resonance (SPR) structures [22–24], and optical waveguides [25–27]. The control of the lateral shift is also of great interest for its practical applications. The nonlinear optical effect [28,29], electrically controlled graphene [30,31], magnetically controlled

crystal [32], and coherent media [33–44] can be utilized to effectively manipulate the GH shift.

A waveguide is widely used to enhance the GH effect [6,7,25–27]. The reflected light beam experiences a large displacement as the guided mode is excited. The magnitude and sign of the lateral shift are related to the internal damping and radiation damping. By adjusting the thickness of the coupling layer, the radiation damping can become larger (smaller) than the internal damping, thereby resulting in a positive (negative) beam shift. In this paper, we present a more convenient way to manipulate the magnitude and sign of the GH shift by tuning the internal damping of a metal-clad waveguide backed by a coherent medium. Based on the atomic coherence and quantum interference effects [45–47], the absorption of the medium can be coherently controlled, thus directly affecting the energy loss of guides modes and the lateral shift. In addition, the width of the resonance dip also depends on the absorption of the medium. Therefore, the angular GH shift can be manipulated as well without changing the structure of the device. Compared with the SPR configurations, where only transverse-magnetic (TM) polarized light suffers a large lateral shift, significantly enhanced GH effect can be simultaneously observed for TM and transverse-electric (TE) waves with the proposed waveguide.

This paper is organized as follows: In Sec. II, we introduce the theoretical model of a metal-clad waveguide backed by a three-level V-type coherent medium, and then we derive the expressions for spatial and angular GH shifts for the reflected light. In Sec. III, we show that guided modes can be excited by both TM- and TE-polarized light, thus resulting in large GH shifts to these beams. In Sec. IV, numerical results and discussions are presented to give a detailed analysis and explanation for the coherent control of spatial and angular GH shifts via adjusting the complex susceptibility of the medium. Finally, we present our conclusions in Sec. V.

*wrg@snnu.edu.cn

†zubairy@physics.tamu.edu

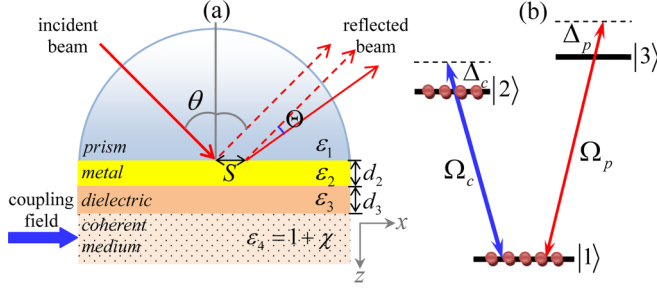


FIG. 1. (a) Schematic of spatial and angular Goos-Hänchen effects in a metal-clad waveguide structure composed of a prism, metal, and a dielectric waveguide. The waveguide is backed by an atomic medium. (b) Three-level V-type atomic system, the absorption and refractivity of which can be coherently controlled.

II. MODEL AND EQUATIONS

We consider a planar four-layer waveguide structure that consists of a prism, a thin metal-cladding with thickness d_2 , a dielectric waveguide with thickness d_3 , and a coherent atomic medium [see Fig. 1(a)]. Their dielectric constants are ϵ_1 , ϵ_2 , ϵ_3 , and ϵ_4 , respectively. The permittivity of the coherent medium can be written as $\epsilon_4 = 1 + \chi$, with χ being the susceptibility. Here, a silver film is utilized as the cladding metal. Light beam is incident upon the prism-silver interface at angle θ and coupled into the waveguide by an evanescent wave when the x -component of the wave vector matches the propagation constant of the guided mode. Meanwhile, a spatial shift S and an angular shift Θ can be found in the reflected beam. The two shifts are related to the complex reflection coefficient of the four-layer structure given by

$$r(\theta) = \frac{r_{12}(1 + r_{23}r_{34}e^{2ik_3d_3}) + (r_{23} + r_{34}e^{2ik_3d_3})e^{2ik_2d_2}}{(1 + r_{23}r_{34}e^{2ik_3d_3}) + r_{12}(r_{23} + r_{34}e^{2ik_3d_3})e^{2ik_2d_2}}, \quad (1)$$

where r_{ij} ($i, j = 1, 2, 3, 4$) represents Fresnel's reflection coefficient between two adjacent layers, which can be expressed as

$$r_{ij} = \begin{cases} \frac{k_{iz}/\epsilon_i - k_{jz}/\epsilon_j}{k_{iz}/\epsilon_i + k_{jz}/\epsilon_j} & \text{for TM polarization,} \\ \frac{k_{iz} - k_{jz}}{k_{iz} + k_{jz}} & \text{for TE polarization.} \end{cases} \quad (2)$$

Here $k_{iz} = k_0(\epsilon_i - \epsilon_1 \sin^2 \theta)^{1/2}$ denotes the normal component of the wave vector in the i th layer. $k_0 = 2\pi/\lambda$ represents the wave vector and λ is the light wavelength. For the incident light beam with a sufficiently large waist (i.e., a narrow angular spectrum $\Delta k \ll k$), the spatial and angular GH shifts of the reflected beam can be written as [24]

$$S = -\frac{\lambda}{2\pi\sqrt{\epsilon_1}} \frac{d\phi}{d\theta} = -\frac{\lambda}{2\pi\sqrt{\epsilon_1}} \text{Im} \left[\frac{d \ln r(\theta)}{d\theta} \right], \quad (3)$$

$$\Theta = \frac{\theta_0^2}{2|r|} \frac{d|r|}{d\theta} = \frac{\theta_0^2}{2} \text{Re} \left[\frac{d \ln r(\theta)}{d\theta} \right], \quad (4)$$

where ϕ refers to the phase of complex reflectivity. Here θ_0 denotes the angular spread of the incident beam, which is inversely proportional to the beam waist.

The excitation of the guided mode depends on the dielectric constant of the medium adjacent to the waveguide layer. As illustrated in Fig. 1(b), we consider a three-level system as the coherent medium. A coupling field with amplitude E_c interacts with the transition $|1\rangle \leftrightarrow |2\rangle$, while the transition $|1\rangle \leftrightarrow |3\rangle$ is coupled by a probe field with amplitude E_p . Then a V-type system is formed. The probe field is incident upon the prism-metal interface, and its evanescent wave interacts with the atoms. The coupling field with a waist much larger than the probe field is incident from the side of the coherent medium. Within the range of the probe light beam, it is covered by a coupling laser with a uniform electric field. Moreover, the coupling field with a Gaussian profile can be reshaped into a flat-top beam that has a uniform distribution of intensity. Under the electric-dipole and rotating-wave approximations, the interaction Hamiltonian of the system is given by

$$H_{\text{int}} = -\hbar[\Delta_c|2\rangle\langle 2| + \Delta_p|3\rangle\langle 3| + (\Omega_c|2\rangle\langle 1| + \Omega_p|3\rangle\langle 1| + \text{H.c.})], \quad (5)$$

where $\Delta_c = \omega_c - \omega_{21}$ and $\Delta_p = \omega_p - \omega_{31}$ are the detunings, and $\Omega_c = \mu_{21}E_c/(2\hbar)$ and $\Omega_p = \mu_{31}E_p/(2\hbar)$ are the Rabi frequencies with μ_{ij} being the electric-dipole moment of transition $|i\rangle \leftrightarrow |j\rangle$. By using the Liouville equation $\dot{\rho} = -(i/\hbar)[H_{\text{int}}, \rho] + L_p$ (L_p represents the relaxation process), we can obtain the equations of motion for the density matrix elements:

$$\begin{aligned} \dot{\rho}_{11} &= i\Omega_c\rho_{21} - i\Omega_c\rho_{12} + i\Omega_p\rho_{31} \\ &\quad - i\Omega_p\rho_{13} + \Gamma_2\rho_{22} + \Gamma_3\rho_{33}, \end{aligned} \quad (6)$$

$$\dot{\rho}_{22} = i\Omega_c\rho_{12} - i\Omega_c\rho_{21} - \Gamma_2\rho_{22}, \quad (7)$$

$$\dot{\rho}_{21} = i\Omega_c\rho_{11} - i\Omega_c\rho_{22} - i\Omega_p\rho_{23} + i(\Delta_c + i\gamma_{21})\rho_{21}, \quad (8)$$

$$\dot{\rho}_{31} = i\Omega_p\rho_{11} - i\Omega_p\rho_{33} - i\Omega_c\rho_{32} + i(\Delta_p + i\gamma_{31})\rho_{31}, \quad (9)$$

$$\dot{\rho}_{32} = i\Omega_p\rho_{12} - i\Omega_c\rho_{31} + i[(\Delta_p - \Delta_c) + i\gamma_{32}]\rho_{31}, \quad (10)$$

where Γ_2 and Γ_3 denote the spontaneous decays from the upper levels $|2\rangle$ and $|3\rangle$. $\gamma_{21} = \Gamma_2/2$, $\gamma_{31} = \Gamma_3/2$, and $\gamma_{32} = (\Gamma_2 + \Gamma_3)/2$ represent the decoherence rates of the relevant transitions, respectively. The above equations are constrained by $\rho_{11} + \rho_{22} + \rho_{33} = 1$ and $\rho_{ij} = \rho_{ji}^*$ ($i \neq j$).

In the limit of a weak probe field ($\Omega_p \ll \Omega_c, \Gamma_2, \Gamma_3$), we can derive the first-order solution of matrix element $\rho_{31}^{(1)}$, which is given by

$$\rho_{31}^{(1)} = -\frac{\Omega_p[(\Delta_p - \Delta_c) + i\gamma_{32}]\rho_{11}^{(0)} + \Omega_p\Omega_c\rho_{12}^{(0)}}{(\Delta_p + i\gamma_{31})[(\Delta_p - \Delta_c) + i\gamma_{32}] - \Omega_c^2}, \quad (11)$$

where the relevant zero-order solutions of matrix elements are

$$\rho_{11}^{(0)} = \frac{1 + \Delta n^{(0)}}{2}, \quad (12)$$

$$\rho_{12}^{(0)} = -\frac{\Omega_c \Delta n^{(0)}}{\Delta_c - i\gamma_{21}}, \quad (13)$$

$$\Delta n^{(0)} = \rho_{11}^{(0)} - \rho_{22}^{(0)} = \frac{1}{1 + \frac{2\Omega_c^2}{\Delta_c^2 + \gamma_{21}^2}}. \quad (14)$$

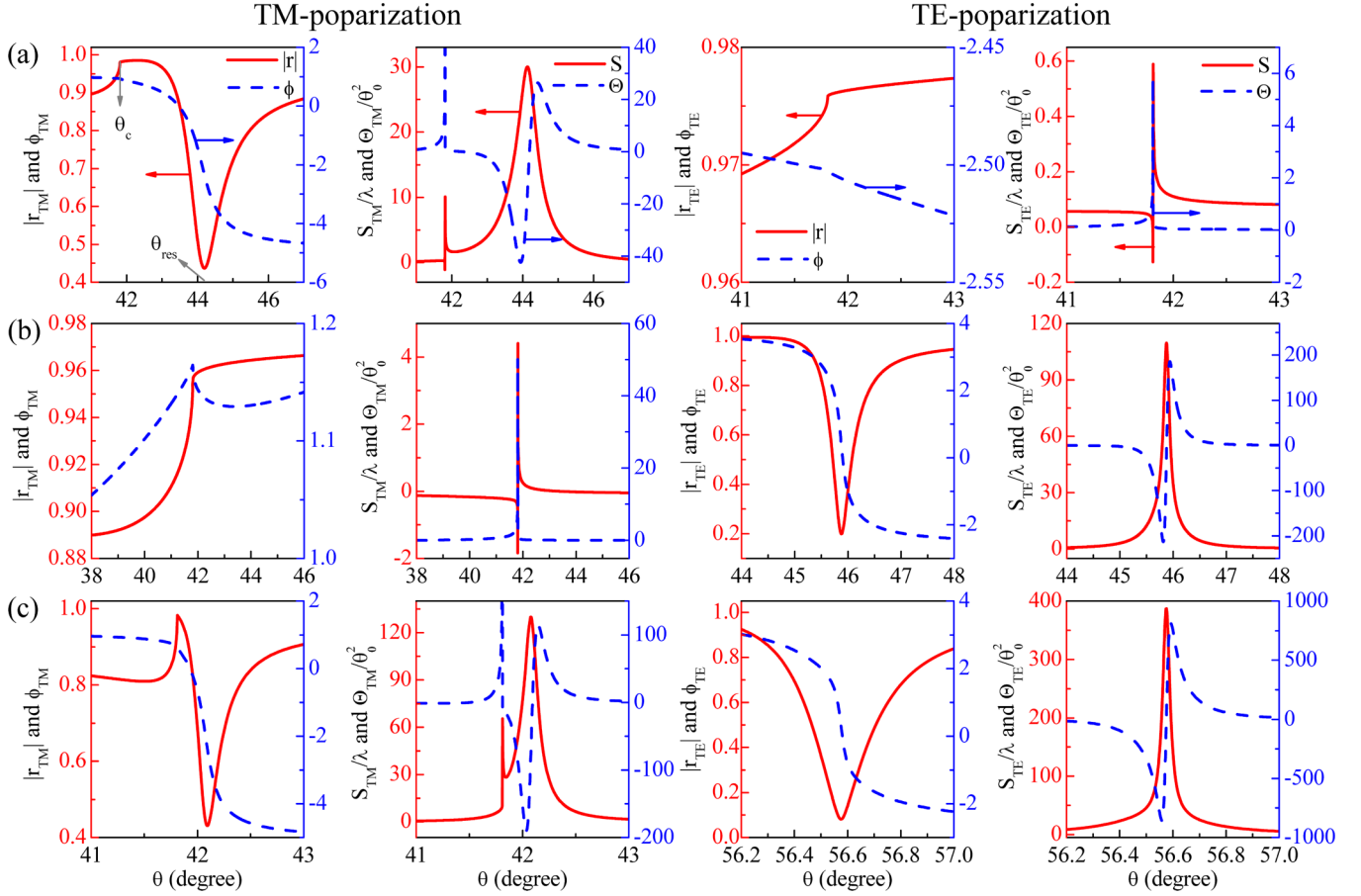


FIG. 2. Reflectivity $|r|$, phase difference ϕ , spatial GH shift S , and angular GH shift Θ as a function of incident angle θ for TM (left two columns) and TE (right two columns) -polarized light with different waveguide thickness. (a) $d_3 = 0$; (b) $d_3 = 0.25\lambda$; (c) $d_3 = 0.4\lambda$. Other parameters are $\varepsilon_1 = 2.25$, $\varepsilon_2 = -13.3 + 0.883i$, $\varepsilon_3 = 2.25$, $\varepsilon_4 = 1$, and $d_2 = 0.06\lambda$.

Considering a cold atomic medium, we neglect the Doppler frequency shifts induced by the thermal motion of atoms. It follows from the atomic polarization, $P = \varepsilon_0 \chi E_p = N \mu_{31} \rho_{31}$, that the linear susceptibility for the probe field is given by

$$\chi(\Delta_p) = -\beta \frac{[(\Delta_p - \Delta_c) + i\gamma_{32}] \rho_{11}^{(0)} + \Omega_c \rho_{12}^{(0)}}{(\Delta_p + i\gamma_{31})[(\Delta_p - \Delta_c) + i\gamma_{32}] - \Omega_c^2}, \quad (15)$$

with $\beta = \mathcal{N} \mu_{31}^2 / (2\hbar \varepsilon_0)$, \mathcal{N} is the atomic density, and ε_0 is the dielectric constant in vacuum. Based on quantum coherence effect, the atomic susceptibility is tunable. This helps in manipulating the resonant modes in the waveguide, and consequently the GH shift.

The V-type system can be realized, for example, with the transitions of the sodium D2 line, the resonant wavelength of which is about 589.1 nm. In numerical calculations, the parameters of the atom are taken to be $\Gamma_2 = \Gamma_3 = 1$ and $\beta = 0.01$. The Rabi frequency and detunings of light fields are scaled by the decay rates.

III. SIMULTANEOUS LARGE GH SHIFT FOR TM AND TE LIGHT BEAMS

For the conventional three-layer Kretschmann structure, a large GH shift can be obtained only for TM-polarized light when SPR is resonantly excited, and there is little lateral shift

for TE-polarized light [22–24]. In this section, we show that large GH spatial shifts can occur simultaneously for TE and TM beams reflected from the metal-clad waveguide.

First, we investigate the influence of waveguide thickness on the lateral displacement in the absence of a coherent medium, i.e., $\varepsilon_4 = 1$. In Fig. 2, we plot the reflectivity, phase difference, and spatial and angular GH shifts versus the incident angle for different values of d_3 . The two columns on the left and the two on the right correspond to the cases of TM- and TE-polarized incident beams, respectively. When a light beam is incident at an angle larger than the critical angle, which is given by $\theta_c = \sin^{-1}(1/\sqrt{\varepsilon_1}) = 41.8^\circ$, the light undergoes total reflection. However, due to the thin metal film, the photon energy can be coupled to the surface plasmon wave or the guided modes when the light beam is incident at the resonance angle θ_{res} . Then a drop appears in the reflectivity. When $d_3 = 0$, we observe a reflection dip near θ_c for the TM wave. At θ_{res} , the reflection phase experiences a sharp variation, which then gives rise to an enhanced spatial displacement [see the left two columns in Fig. 2(a)]. Nevertheless, the TE wave is almost totally reflected by the layered structure, and the change of phase is extremely small. Therefore, there are only small spatial and angular shifts at θ_c [see the right two columns in Fig. 2(a)]. As the waveguide thickness d_3 is increased to $d_3 = 0.25\lambda$, the results are opposite to the

above case [see Fig. 2(b)]. The TM wave is totally reflected with small lateral and angular shifts at θ_c , while the TE wave is laterally displaced and deflected in the sharp dip where reflectivity is dramatically reduced [see Fig. 2(b)]. When we further increase the thickness to $d_3 = 0.4\lambda$, a resonance dip can be obtained for both TM- and TE-polarized light beams, respectively [see Fig. 2(c)]. Compared to Figs. 2(a) and 2(b), the angular widths of these dips are narrowed and the reflection phases change more sharply. As a result, enhanced spatial and angular GH effects can simultaneously be observed for TM and TE waves incident around their resonance angles. The direction of the lateral displacement is related to the sign of $d\phi/d\theta$. In these cases, ϕ_{TM} and ϕ_{TE} decrease with the incident angle in the reflection dips, i.e., $d\phi/d\theta < 0$. Therefore, the reflected beam undergoes a positive shift with respect to the incident point.

When light is incident on the prism-metal interface with an angle larger than θ_c , total internal reflection occurs. If the resulting evanescent wave couples resonantly to the waveguide, certain guided modes can be excited accompanied by sharply decreasing reflection. Then the energy penetrates into the waveguide. The criterion for the four-layer waveguide mode can be written as [48]

$$\varphi_3 + \varphi_{321} + \varphi_{34} = 2\pi m, \quad (16)$$

with

$$\varphi_3 = 2k'_{3z}d_3, \quad (17)$$

$$\varphi_{321} = 2 \tan^{-1} \left[i \left(\frac{1 - r'_{32}}{1 + r'_{32}} \right) \left(\frac{1 - r'_{21} e^{2ik'_{2z}d_2}}{1 + r'_{21} e^{2ik'_{2z}d_2}} \right) \right], \quad (18)$$

$$\varphi_{34} = 2 \tan^{-1} \left[i \left(\frac{\varepsilon_3}{\varepsilon_4} \right)^\eta \left(\frac{k'_{4z}}{k'_{3z}} \right) \right], \quad (19)$$

$$k'_{iz} = \pm k_0 \sqrt{\varepsilon_i - N^2} \quad (i = 1, 2, 3, 4), \quad (20)$$

$$r'_{ij} = \frac{\varepsilon_j^\eta k'_{iz} - \varepsilon_i^\eta k'_{jz}}{\varepsilon_j^\eta k'_{iz} + \varepsilon_i^\eta k'_{jz}}, \quad (21)$$

where $m = 0, 1, 2, \dots$ represents the mode index, φ_3 is the phase shift of light propagating in the waveguide, and φ_{321} and φ_{34} refer to the phase shifts experienced by the light due to reflections at the waveguide-metal-prism and waveguide-medium boundaries, respectively. Here $\eta = 0, 1$ correspond to the cases of TE- and TM-polarized incident lights, respectively. The complex number $N = N' + iN''$ is due to the absorption of metal and the medium. In Fig. 3, we plot the effective refractive index N' versus the waveguide thickness d_3 for $m = 0, 1, 2$. Mode resonances take place at certain angles determined by $N' = \sqrt{\varepsilon_1} \sin \theta_{\text{res}}$, thus leading to attenuated total reflection. It is clear that the resonance angle θ_{res} of all modes increases with d_3 . When the waveguide is relatively thin, only the TM_0 mode can be excited with a dip in reflectance [see Fig. 2(a)]. This refers to the well-known SPR. As d_3 increases, the resonance angle of the SPR mode increases to 90° and then disappears. Meanwhile, the first guided mode, i.e., the TE_0 mode, starts to exist when d_3 is larger than the cutoff thickness. Under the condition of cutoff thickness, the effective refractive index is $N' = 1$ and the

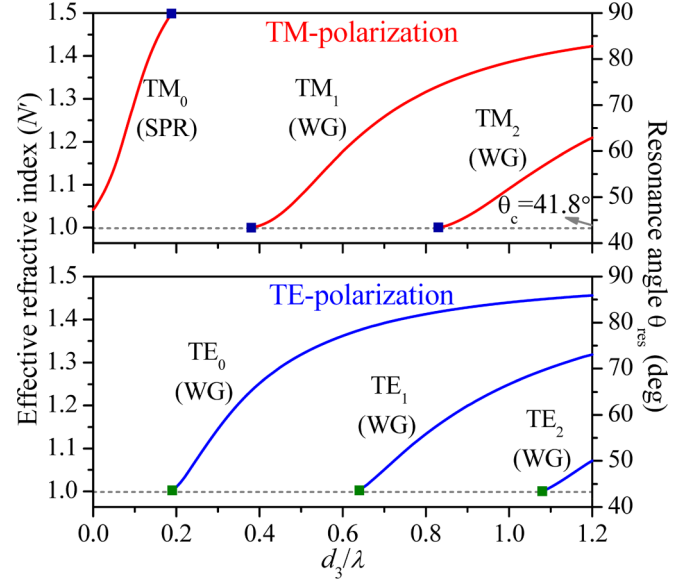


FIG. 3. Dependence of effective refractive index N' and resonance angle θ_{res} of the mode resonance on the waveguide thickness for TM- and TE-polarized light. The squares denote the cutoff thickness of the waveguide for different modes. Parameters are the same as those in Fig. 2.

resonance angle θ_{res} is equal to the critical angle θ_c . If d_3 is increased further, more waveguide modes can be excited. The reflection dips in Figs. 2(b) and 2(c) correspond to the TE_0 and TM_1 modes. It is obvious that the angular width of the guided mode is much narrower than that of the SPR mode, and therefore the phase difference between the incident and the reflected light changes more sharply around the resonance angle. Comparing with Fig. 2(a), we can see that the spatial GH shifts are significantly enhanced for the waveguide modes. Meanwhile, the angular GH effect can be enhanced as well due to the narrow reflection spectrum.

IV. TUNABLE GIANT GH SHIFT VIA A COHERENT MEDIUM

As mentioned above, enhanced spatial and angular GH shifts can be simultaneously achieved for TM and TE beams when attenuated total reflection occurs. As the resonance of the guided mode is sensitive to the dielectric constant of the medium, we are able to manipulate the spatial and angular beam shifts by controlling the atomic susceptibility.

First, we consider the control of the spatial GH shift by the coupling field. The reflectivity $|r|$, the phase difference ϕ , and the lateral displacement S versus the incident angle θ for different control field Rabi frequency Ω_c are illustrated in Fig. 4. Figures 4(a1)–4(a3) and 4(b1)–4(b3) correspond to the cases of TM and TE polarizations, respectively. We see that a large spatial GH shift arises at the resonance angle of guided mode (θ_{res}), where there is a great reduction in reflection. Within the dip, ϕ suffers a distinct sharp variation in the vicinity of θ_{res} . When Ω_c is increased, the reflection dip becomes narrow initially and then broadens, and the variation of ϕ is steeper for narrow dips. As a result, the magnitude of lateral displacement is increased initially and

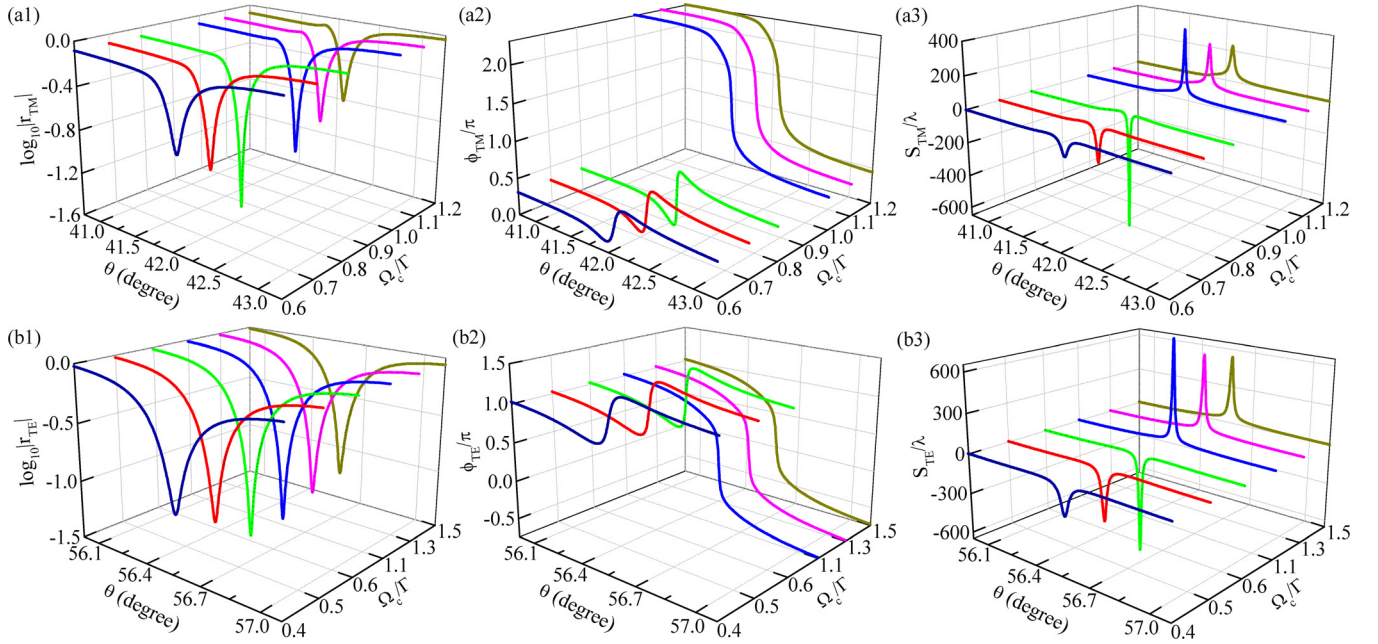


FIG. 4. Reflectivity $|r|$, phase difference ϕ , and spatial Goos-Hänchen shift S as a function of incident angle θ for different coupling-field Rabi frequency Ω_c . (a1) $|r_{TM}|$, (a2) ϕ_{TM} , (a3) S_{TM} ; (b1) $|r_{TE}|$, (b2) ϕ_{TE} , (b3) S_{TE} . Parameters are $\Gamma_2 = \Gamma_3 = 1$, $\beta = 0.01$, $\Delta_p = 0$, and $\Delta_c = 0$. Other parameters are the same as those in Fig. 2(c).

then decreased. However, its direction switches from negative to positive with respect to the geometric reflection point. The sign is determined by the slope of the curve of ϕ versus θ where a positive (negative) gradient corresponds to a negative (positive) lateral shift.

For the four-layer prism-waveguide coupling system, the spatial GH shift at θ_{res} can be written as [25]

$$S = \frac{2\Gamma_{rad}}{\Gamma_{rad}^2 - \Gamma_{int}^2} \cos \theta_{res}. \quad (22)$$

Here, Γ_{int} represents the internal damping of a three-layer metal-waveguide-medium structure that originates from the intrinsic absorption losses of metal and medium. As a prism is coupled to the waveguide, a four-layer structure is formed and additional loss arises due to the thin metal layer. Here

Γ_{rad} represents the backscattered radiation damping from the metal film and is inversely proportional to the exponential function of d_2 . Nevertheless, Γ_{int} is sensitive to the absorption coefficient of the medium. Therefore, the transition between negative and positive lateral shifts can be controlled by the imaginary part of the susceptibility of the coherent atoms.

In Fig. 5, we plot the susceptibility of the medium, the dip minimum of reflectivity, and the peak value of the GH shift as a function of Ω_c . In the case of two-photon resonance, i.e., $\Delta_p = \Delta_c$, the real part of the susceptibility is zero. Under the drive of a coupling field, the ground state $|1\rangle$ splits into two dressed levels $|\pm\rangle = (|1\rangle \mp |2\rangle)/\sqrt{2}$ with eigenenergies $E_{\pm} = \pm\Omega_c$. The splitting increases with Ω_c , thereby leading to the decrease of probe absorption [see Fig. 5(a)]. Consequently, the internal damping Γ_{int} is reduced monotonically. It changes

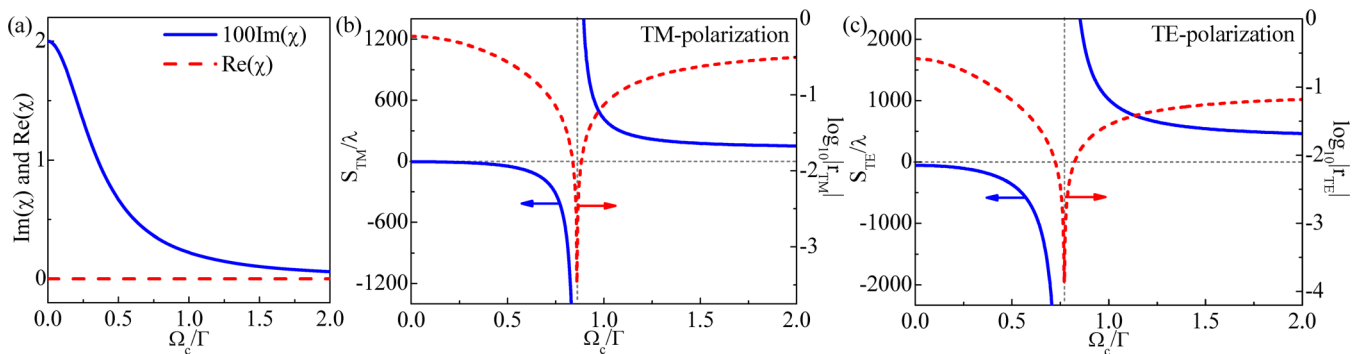


FIG. 5. (a) Probe susceptibility vs coupling-field Rabi frequency Ω_c . Reflectivity $|r|$ (dashed line) and spatial GH shift S (solid line) at resonant angle θ_{res} as a function of Ω_c : (b) TM-polarized light, (c) TE-polarized light. Parameters are the same as those in Fig. 4.

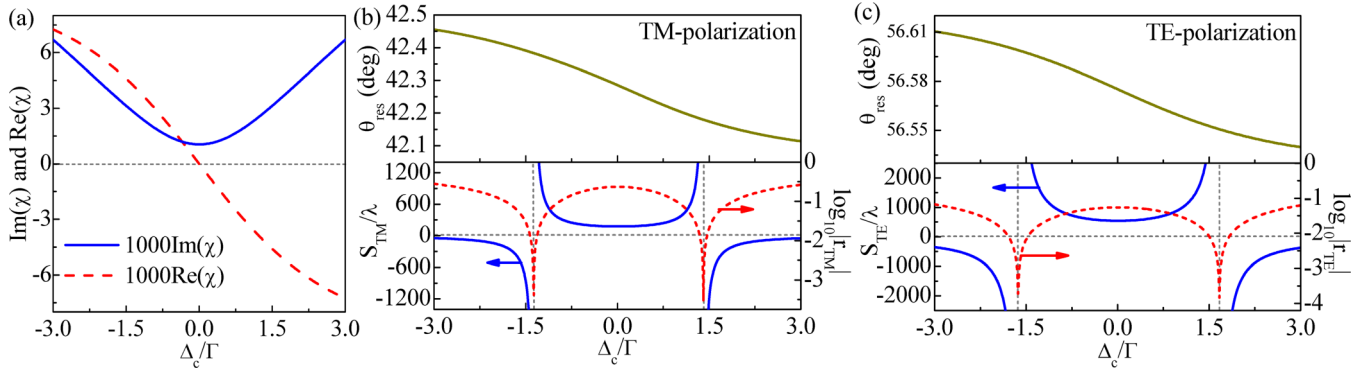


FIG. 6. (a) Probe susceptibility vs coupling-field detuning Δ_c . Dependence of $|r|$ (dashed line) and S (solid line) at resonant angle θ_{res} on Δ_c : (b) TM-polarized light, (c) TE-polarized light. Parameters are $\Delta_p = 0$ and $\Omega_c = 1.5$. Other parameters are the same as those in Fig. 2(c).

from the case of $\Gamma_{\text{int}} > \Gamma_{\text{rad}}$ to $\Gamma_{\text{int}} < \Gamma_{\text{rad}}$. As a result, the direction of lateral displacement is switched from negative to positive. When Γ_{int} is close to Γ_{rad} , a giant spatial shift can be observed for TM- and TE-polarized beams accompanied by large attenuation in reflection [see Figs. 5(b) and 5(c)]. The two dampings become equal at an optimal value of Ω_c where the phase difference ϕ undergoes an abrupt change. Then the spatial GH shift becomes infinite. Nevertheless, ϕ has no physical meaning in this case.

According to Eq. (15), the susceptibility also depends on the detuning of the coupling field, which can then be used to manipulate the lateral shift. The susceptibility, resonance angle, reflection minimum, and peak value of the GH shift as a function of Δ_c are shown in Fig. 6. In the case of $\Delta_c \neq \Delta_p$, the two-photon resonance condition is not fulfilled. The probe absorption increases with $|\Delta_c|$ and the refractive index [$n \approx 1 + \text{Re}(\chi)/2$] decreases monotonically with Δ_c as depicted in Fig. 6(a). There are two optimal values of Δ_c above (below) which the sign of the lateral shift changes. The internal damping is less than the radiation damping for small $|\Delta_c|$. In this case, we obtain a positive spatial GH shift whose magnitude increases with $|\Delta_c|$, while for large $|\Delta_c|$ the internal damping becomes larger than the radiation damping, and a negative lateral shift occurs that decreases with $|\Delta_c|$. Enhanced spatial GH effect can also be achieved around certain values of field detuning where the reflection is extremely attenuated [see Figs. 6(b) and 6(c)]. The change of refractive index has very little influence on the internal

damping. However, it strongly affects the resonance angle. With the increase of Δ_c , θ_{res} varies almost linearly with $\text{Re}(\chi)$. Therefore, the peak position of the spatial GH shift can be tuned as well by adjusting the detuning.

Next, we investigate the control of the angular GH effect via the coherent medium. We plot Θ as a function of θ for different values of Ω_c in Fig. 7. It can be seen that the angular GH shift is extremely large near the resonance angle, while its sign has a sudden change. According to Eq. (4), the angular GH shift is proportional to the slope of the reflectivity curve versus θ and inversely proportional to $|r|$. A sharp reflection dip with low reflectivity can give rise to a significant enhancement of Θ . Therefore, initially the magnitude of Θ increases with Ω_c and then decreases gradually. Its change is related to the angular width of the reflection spectrum. In particular, the value of Θ is exactly zero at θ_{res} since the derivative $d|r|/d\theta = 0$. Compared with the case in Fig. 4 where the sign of the spatial GH shift is switched at a certain value of Ω_c , the sign of Θ does not change with Ω_c . As mentioned in Fig. 2, the resonance dips for guided modes are much narrower than that of the SPR mode, and a large angular GH shift is obtained by using the waveguide resonance. Moreover, Θ can also be modulated by the detuning Δ_c . The corresponding results are illustrated in Fig. 8. It is obvious that the angular GH effect can be enhanced simultaneously for TM- and TE-polarized beams incident at different angles. In addition, the angular width of the resonance dip of the TE mode is narrower than that of the TM mode, thereby resulting in a large angular beam shift.

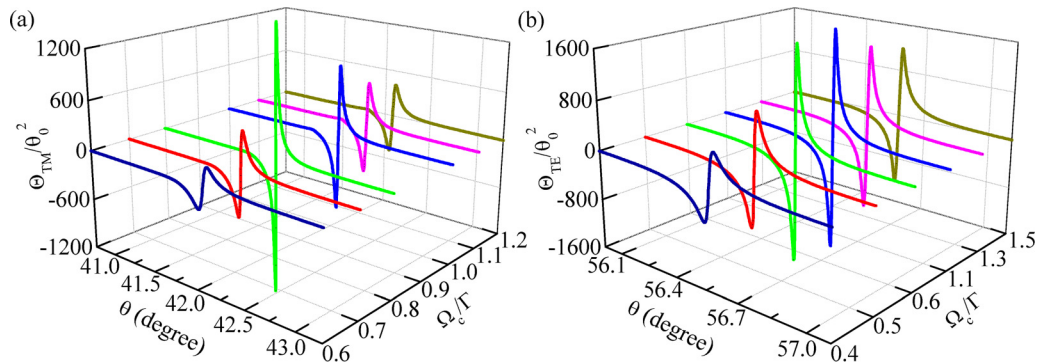


FIG. 7. Angular Goos-Hänchen shift Θ as a function of incident angle θ for different coupling-field intensity Ω_c . (a) TM-polarized light, (b) TE-polarized light. Other parameters are the same as those in Fig. 4.

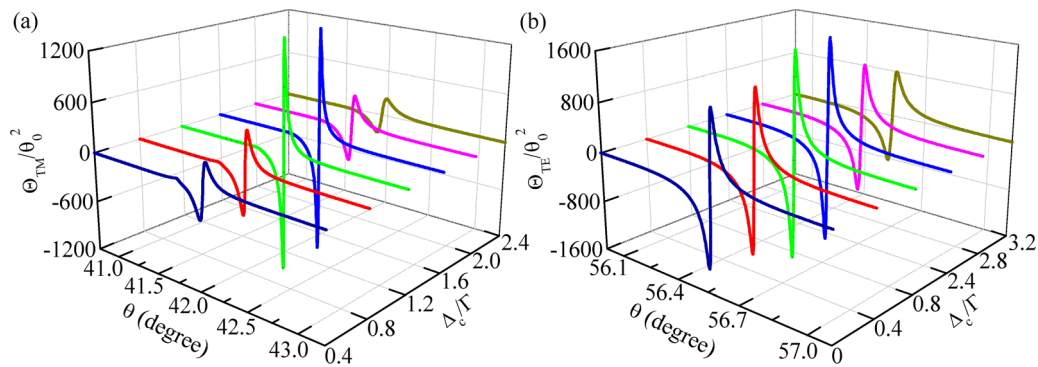


FIG. 8. Angular Goos-Hänchen shift Θ as a function of incident angle θ for different coupling-field detuning Δ_c . (a) TM-polarized light, (b) TE-polarized light. Other parameters are the same as those in Fig. 6.

V. CONCLUSION

In conclusion, we have proposed a scheme to manipulate the spatial and angular GH effects of a reflected light beam from a metal-clad waveguide backed by a V-type coherent atomic medium. By tuning the thickness of the waveguide layer, guided mode resonance can be excited simultaneously for TM and TE waves incident at different angles, thereby resulting in significant lateral displacement and angular deflection in the resonance dips. The magnitude and sign of the spatial GH shift are dependent on the internal and radiation dampings of the system. By adjusting the absorption of the medium, the internal damping can be controlled coherently, and we can obtain giant positive and negative lateral beam shifts. In addition, the resonance angle as well as the peak position of the spatial GH shift can be tuned by the refractive index of the medium. For certain values of atomic absorption, the reflection is strongly suppressed and the resonance dips of the guided mode become quite sharp and narrow. Therefore,

an enhanced angular GH effect can be observed. Compared to other schemes where the beam shifts are controlled by the thickness of a metal layer, we are able to modulate the GH effects more conveniently and in a flexible manner without changing the system structure. Our study indicates that other well-investigated coherent media, namely solid crystals and quantum wells, can also be utilized to manipulate the spatial and angular beam shifts.

ACKNOWLEDGMENTS

This work was supported by the Natural National Science Foundation of China (NSFC) (Grant No. 11204367), Natural Science Basic Research Plan in Shaanxi Province (Grant No. 2018JQ1051), Fundamental Research Funds for the Central Universities (GK202003021), and the Scholarship Program of China Scholarship Council (Grant No. 201806875036). This work is also supported by a grant from King Abdulaziz City for Science and Technology (KACST).

- [1] F. Goos and H. Hänchen, Ein neuer und fundamentaler versuch zur totalreflexion, *Ann. Phys.* **436**, 333 (1947).
- [2] K. Artmann, Berechnung der seitenversetzung des totalreflektierten strahles, *Ann. Phys.* **437**, 87 (1948).
- [3] M. A. Porrás, Moment-method evaluation of the angular and lateral shifts of reflected light beams, *Opt. Commun.* **131**, 13 (1996).
- [4] M. Merano, A. Aiello, M. P. van Exter, and J. P. Woerdman, Observing angular deviations in the specular reflection of a light beam, *Nat. Photon.* **3**, 337 (2009).
- [5] T. Sakata, H. Togo, and F. Shimokawa, Reflection-type 2×2 optical waveguide switch using Goos-Hänchen effect, *Appl. Phys. Lett.* **76**, 2841 (2000).
- [6] Y. Wang, H. Li, Z. Cao, T. Yu, Q. Shen, and Y. He, Oscillating wave sensor based on the Goos-Hänchen effect, *Appl. Phys. Lett.* **92**, 061117 (2008).
- [7] T. Yu, H. Li, Z. Cao, Y. Wang, Q. Shen, and Y. He, Oscillating wave displacement sensor using the enhanced Goos-Hänchen effect in a symmetrical metal-cladding optical waveguide, *Opt. Lett.* **33**, 1001 (2008).
- [8] C. W. Chen, W. C. Lin, L. S. Liao, Z. H. Lin, H. P. Chiang, P. T. Leung, E. Sijercic, and W. S. Tse, Optical temperature sensing based on the enhanced Goos-Hänchen effect, *Appl. Opt.* **46**, 5347 (2007).
- [9] A. Kar, N. Goswami, and A. Saha, Analysis of high-resolution electro-optical beam steering by long-range surface plasmon resonance using a ZnSe prism, *Appl. Opt.* **56**, 9656 (2017).
- [10] R. Talebzadeh and A. Namdar, Positively and negatively large Goos-Hänchen lateral displacements from a single negative layered structure, *Appl. Opt.* **51**, 6484 (2012).
- [11] R. W. Ziolkowski, Pulsed and CW Gaussian beam interactions with double negative metamaterial slabs, *Opt. Express* **11**, 662 (2003).
- [12] L. G. Wang and S. Y. Zhu, Large negative lateral shifts from the Kretschmann-Raether configuration with left-handed materials, *Appl. Phys. Lett.* **87**, 221102 (2005).
- [13] C. F. Li, Negative Lateral Shift of a Light Beam Transmitted Through a Dielectric Slab and Interaction of Boundary Effects, *Phys. Rev. Lett.* **91**, 133903 (2003).

- [14] L. G. Wang, H. Chen, and S. Y. Zhu, Large negative Goos-Hänchen shift from a weakly absorbing dielectric slab, *Opt. Lett.* **30**, 2936 (2005).
- [15] H. M. Lai and S. W. Chan, Large and negative Goos-Hänchen shift near the Brewster dip on reflection from weakly absorbing media, *Opt. Lett.* **27**, 680 (2002).
- [16] Y. Yan, X. Chen, and C. F. Li, Large and negative lateral displacement in an active dielectric slab configuration, *Phys. Lett. A* **361**, 178 (2007).
- [17] D. Felbacq, A. Moreau, and R. Smaïli, Goos-Hänchen effect in the gaps of photonic crystals, *Opt. Lett.* **28**, 1633 (2003).
- [18] V. Soboleva, V. V. Moskalenko, and A. A. Fedyanin, Giant Goos-Hänchen Effect and Fano Resonance at Photonic Crystal Surfaces, *Phys. Rev. Lett.* **108**, 123901 (2012).
- [19] Y. Chen, Y. Ban, Q. B. Zhu, and X. Chen, Graphene-assisted resonant transmission and enhanced Goos-Hänchen shift in a frustrated total internal reflection configuration, *Opt. Lett.* **41**, 4468 (2016).
- [20] R. U. Din, X. D. Zeng, I. Ahmad, and G. Q. Ge, Enhanced and highly tunable Goos-Hänchen shifts at a nanocomposite-graphene interface, *Appl. Phys. Lett.* **114**, 161902 (2019).
- [21] C. F. Li and Q. Wang, Prediction of simultaneously large and opposite generalized Goos-Hänchen shifts for TE and TM light beams in an asymmetric double-prism configuration, *Phys. Rev. E* **69**, 055601(R) (2004).
- [22] X. B. Yin, L. Hesselink, Z. W. Liu, N. Fang, and X. Zhang, Large positive and negative lateral optical beam displacements due to surface plasmon resonance, *Appl. Phys. Lett.* **85**, 372 (2004).
- [23] L. Chen, X. B. Liu, Z. Q. Cao, and S. L. Zhuang, Mechanism of giant Goos-Hänchen effect enhanced by long-range surface plasmon excitation, *J. Opt.* **13**, 035002 (2011).
- [24] L. Salasnich, Enhancement of four reflection shifts by a three-layer surface-plasmon resonance, *Phys. Rev. A* **86**, 055801 (2012).
- [25] X. B. Liu, Z. Q. Cao, P. F. Zhu, Q. S. Shen, and X. M. Liu, Large positive and negative lateral optical beam shift in prism-waveguide coupling system, *Phys. Rev. E* **73**, 056617 (2006).
- [26] L. Chen, Z. Q. Cao, F. Ou, H. G. Li, Q. H. Shen, and H. C. Qiao, Observation of large positive and negative lateral shifts of a reflected beam from symmetrical metal-cladding waveguides, *Opt. Lett.* **32**, 1432 (2007).
- [27] X. M. Liu, Q. F. Yang, Z. Qiao, T. K. Li, P. F. Zhu, and Z. Q. Cao, Physical origin of large positive and negative lateral optical beam shifts in prism-waveguide coupling system, *Opt. Commun.* **283**, 2681 (2010).
- [28] H. C. Zhou, X. Chen, P. Hou, and C. F. Li, Giant bistable lateral shift owing to surface-plasmon excitation in Kretschmann configuration with a Kerr nonlinear dielectric, *Opt. Lett.* **33**, 1249 (2008).
- [29] P. Hou, Y. Y. Chen, X. Chen, J. L. Shi, and Q. Wang, Giant bistable shifts for one-dimensional nonlinear photonic crystals, *Phys. Rev. A* **75**, 045802 (2007).
- [30] L. Y. Jiang, Q. K. Wang, Y. J. Xiang, X. Y. Dai, and S. C. Wen, Electrically tunable Goos-Hänchen shift of light beam reflected from a graphene-on-dielectric surface, *IEEE Photon. J.* **5**, 6500108 (2013).
- [31] X. D. Zeng, M. Al-Amri, and M. S. Zubairy, Tunable Goos-Hänchen shift from graphene ribbon array, *Opt. Express* **25**, 23579 (2017).
- [32] W. J. Yu, H. Sun, and L. Gao, Magnetic control of Goos-Hänchen shifts in a yttrium-iron-garnet film, *Sci. Rep.* **7**, 45866 (2017).
- [33] L. G. Wang, M. Ikram, and M. S. Zubairy, Control of the Goos-Hänchen shift of a light beam via a coherent driving field, *Phys. Rev. A* **77**, 023811 (2008).
- [34] Ziauddin, S. Qamar, and M. S. Zubairy, Coherent control of the Goos-Hänchen shift, *Phys. Rev. A* **81**, 023821 (2010).
- [35] Ziauddin and S. Qamar, Gain-assisted control of the Goos-Hänchen shift, *Phys. Rev. A* **84**, 053844 (2011).
- [36] Ziauddin and S. Qamar, Control of the Goos-Hänchen shift using a duplicated two-level atomic medium, *Phys. Rev. A* **85**, 055804 (2012).
- [37] W. W. Deng, S. P. Wu, and G. X. Li, Enhancement of the Goos-Hänchen shift by electromagnetically induced transparency with amplification, *Opt. Commun.* **285**, 2668 (2012).
- [38] H. R. Hamed, A. Radmehr, and M. Sahrai, Manipulation of Goos-Hänchen shifts in the atomic configuration of mercury via interacting dark-state resonances, *Phys. Rev. A* **90**, 053836 (2014).
- [39] Ziauddin, Y. L. Chuang, and R. K. Lee, Giant Goos-Hänchen shift using PT symmetry, *Phys. Rev. A* **92**, 013815 (2015).
- [40] W. X. Yang, S. P. Liu, Z. H. Zhu, Ziauddin, and R. K. Lee, Tunneling-induced giant Goos-Hänchen shift in quantum wells, *Opt. Lett.* **40**, 3133 (2015).
- [41] X. J. Zhang, H. H. Wang, Z. P. Liang, Y. Xu, C. B. Fan, C. Z. Liu, and J. Y. Gao, Goos-Hänchen shift in a standing-wave-coupled electromagnetically-induced-transparency medium, *Phys. Rev. A* **91**, 033831 (2015).
- [42] S. Asiri, J. Xu, M. Al-Amri, and M. S. Zubairy, Controlling the Goos-Hänchen and Imbert-Fedorov shifts via pump and driving fields, *Phys. Rev. A* **93**, 013821 (2016).
- [43] G. Solookinejad, M. Jabbari, M. Nafar, E. Ahmadi, and S. H. Asadpour, Controlling Goos-Hänchen shifts due to the surface plasmon effect in a hybrid system, *Appl. Opt.* **57**, 8193 (2018).
- [44] T. Shui, W. X. Yang, Q. Y. Zhang, X. Liu, and L. Li, Squeezing-induced giant Goos-Hänchen shift and hypersensitized displacement sensor in a two-level atomic system, *Phys. Rev. A* **99**, 013806 (2019).
- [45] S. E. Harros, Electromagnetically induced transparency, *Phys. Today* **50**(7), 36 (1997).
- [46] M. Fleischhauer, A. Imamoglu, and J. P. Marangos, Electromagnetically induced transparency: Optics in coherent media, *Rev. Mod. Phys.* **77**, 633 (2005).
- [47] M. O. Scully and M. S. Zubairy, *Quantum Optics* (Cambridge University Press, Cambridge, England, 1997).
- [48] N. Skivesen, R. Horvath, and H. C. Pedersen, Optimization of metal-clad waveguide sensors, *Sens. Actuators B* **106**, 668 (2005).